PHYSICAL REVIEW B **89**, 081301(R) (2014)

Optical in-plane anisotropy of ZnO/(Zn,Mg)O quantum wells grown on *a*-plane sapphire: Implications for optical spin control

J. Puls, S. Sadofev, P. Schäfer, and F. Henneberger*

Institut für Physik, Humboldt-Universität zu Berlin, Newtonstrasse 15, 12489 Berlin, Germany

(Received 26 August 2013; revised manuscript received 9 December 2013; published 5 February 2014)

Utilizing the anisotropic thermal expansion of *a*-plane sapphire, we study the role of anisotropic in-plane strain on ZnO quantum well structures. X-ray data reveal a deformation of the hexagonal unit cell. The symmetry reduction shows up in the optical spectra by distinct linear-polarization features, both for the neutral and charged exciton transition. We elaborate the excitonic fine structure behind this observation, accounting for spin-orbit coupling and electron-hole exchange in the presence of anisotropic strain. The consequences for optical spin control are discussed.

DOI: 10.1103/PhysRevB.89.081301 PACS number(s): 71.35.Pq, 73.21.Fg, 78.66.Hf, 85.75.−d

The present interest in ZnO and its nanostructures is not only motivated by possible applications in transparent electronics and optoelectronics [1], but also by the expectation that these systems represent well-suited candidates for spintronics or even quantum computing. In particular, the prediction of room-temperature ferromagnetism for ZnO when doped with magnetic transition metal ions [2] has triggered ongoing research in this field. A further advantage related to the intrinsic ZnO band structure is the weak spin-orbit (SO) interaction that principally favors long spin life and coherence times of the charge carriers. For example, only the D'yakonov-Perel' mechanism is expected to contribute significantly to the spin relaxation of the electrons in *n*-type ZnO [3,4], since the Elliot-Yafet mechanism is strongly weakened by the combination of large band-gap energy and small SO coupling. In many studies, the spin polarization is created by optical pumping with polarized light utilizing the characteristic selection rules of the semiconductor's band-to-band transitions. These selection rules directly mirror the symmetry of the crystal lattice. In heterostructures, the symmetry is often lower than in the bulk crystal as a result of strain inherent to the growth process. As a consequence, selection rules are softened and the spin imprint becomes less perfect. In what follows, we demonstrate this effect for a ZnO/ZnMgO quantum well (QW) as the most frequently studied ZnO-based heterostructure. Generally, when the wave vector $\vec{k}$ of the light is along the hexagonal axis of the wurtzite crystal, only hole states with a definite orbital momentum couple to the radiation field, resulting in completely circularly polarized transitions [5]. However, a remarkable linear polarization of the photoluminescence (PL) is surprisingly found if the QW structure is grown on an *a*-plane sapphire substrate. This approach, also called uniaxially locked epitaxy [6], allows for avoiding orientational domains often found for growth on *c*-plane sapphire and reduces the lattice mismatch. The resultant geometry [see Fig. 1(a)] is such that the hexagonal axes of the substrate ($\vec{c}_S$) and heterostructure ($\vec{c}$) are perpendicular to each other [7]. The characteristic anisotropy of this growth configuration is revealed by probing it with both the neutral (X) and negatively charged (X^-) exciton transition of integer and half-integer spins, respectively, and conclusions with respect to the optical spin control are drawn. The case of X^- is of particular interest since that optical transition is widely used to pump and control the spin of resident electrons as well as nuclear spins in low-dimensional heterostructures such as QWs and quantum dots [8,9].

The samples are grown on *a*-plane sapphire substrates by radical-source molecular beam epitaxy [10]. First, a 30-nm (Zn,Mg)O nucleation layer is grown at 300 °C, followed by an annealing step at 580 °C. The subsequent 600-nm ZnMgO buffer layer is grown at 350 °C. The exemplary multiple QW (MQW) structure studied below is deposited on this composite buffer and consists of seven well-barrier periods. Well and barrier widths are $d_w = 3.7$ and $d_b = 11$ nm, respectively, and the Mg content in the buffer and the barriers amounts to $x_{\mathrm{Mg}} = 0.11$. Finally, an annealing step at 570 °C is applied to the complete sample. From the occurrence of a blue-green deep level emission around 2.5 eV, it can be concluded that the specimen is *n* type, probably through oxygen vacancies [11] formed under metal-rich growth conditions. The growth procedure and structural design are critical for obtaining smooth well/barrier interfaces and practically field-free QWs exhibiting well-resolved X and X^- transitions with an inhomogeneous broadening of clearly less than 10 meV.

The lattice properties of the (Zn,Mg)O buffer and thus of the pseudomorphically grown MQW are studied by x-ray measurements using the Fewster method [12] with a four-crystal, four-reflection Ge monochromator and a two-crystal, three-reflection Ge analyzer. The sample's optical transmission is studied by means of a halogen tungsten lamp with a UG11 color filter to block the intense visible range. Excitation of the PL with tunable photon energy is performed by the frequency-doubled output of a mode-locked pyridine 2 dye laser synchronously pumped by the second harmonic of a mode-locked Nd:YVO_4 laser. PL and transmission spectra are recorded by a spectrometer with 0.5 nm/mm linear dispersion in combination with a liquid-nitrogen-cooled CCD detector.

The room-temperature x-ray analysis shows that the lattice constants *a* and *b* of the hexagonal (Zn,Mg)O unit cell possess practically identical values of $a = (0.325\,480 \pm 0.000\,007)$ nm and $b = 0.325\,475 \pm 0.000\,007$ nm and that the angles to the *c* axis remain at $\alpha = \beta = 90°$. However, a significant deviation from the hexagonal structure is found for the angle $\gamma = (120.017 \pm 0.0013) \neq 120°$, as sketched in Fig. 1(b). The long axis of the stretched hexagon is along $\vec{c}_S$. Therefore, the symmetry of the epitaxial structure is lowered to monoclinic.

*fh@physik.hu-berlin.de

 ©2014 American Physical Society

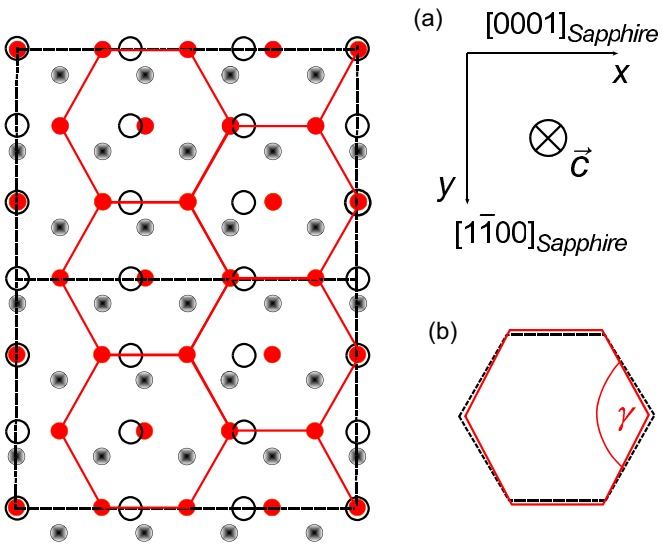

FIG. 1. (Color online) (a) Scheme of (Zn,Mg)O epitaxy on *a*-plane sapphire. Open circles: Positions of O atoms of the top sapphire layer. Solid (red) and dashed gray balls: Zn(Mg) atoms and O atoms, respectively, of (Zn,Mg)O. The hexagonal axis of (Zn,Mg)O $\vec{c}$ points into the plane of drawing. (b) Dashed (black) and solid (red) hexagons: Scheme of the undisturbed and strained, respectively, hexagonal (Zn,Mg)O cell. The same deformation applies for the pseudomorphically grown ZnO QWs. For using the Bir-Pikus Hamiltonian [17] in its standard version, the QW in-plane axes x and y are introduced parallel and perpendicular to $\vec{c}_S$, respectively.

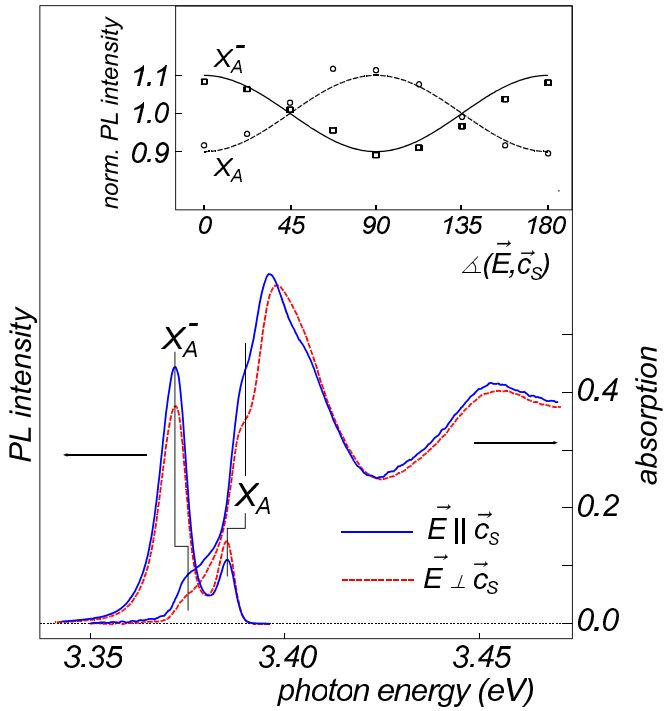

FIG. 2. (Color online) PL (scaled on the left-hand side axis) and absorption (scaled on the right-hand side axis) spectra of a ZnO/(Zn,Mg)O MQW for linear light polarization along $\vec{c}_S$ [solid (blue) lines] and perpendicular to $\vec{c}_S$ [dashed (red) lines]. The spectral position of the lowest neutral exciton state (X_A) and charged exciton state (X_A^-) are marked in the PL and absorption spectra. The absorbance is derived from the measured transmission and reflectivity. To avoid optical alignment in the PL, the MQW is excited by unpolarized light energetically above the band gap of the (Zn,Mg)O barrier ($\hbar\omega_{\mathrm{exc}} = 3.62$ eV). The sample temperature is $T = 5$ K. Inset: Normalized PL intensity of charged (squares) and neutral exciton (circles), respectively, vs the angle between the light polarization vector $\vec{E}$ and $\vec{c}_S$. The lines are used to guide the eyes.

This symmetry reduction is confirmed on a set of differently designed single QW and MQW structures, all grown by the same procedure and all exhibiting the same angles γ and orientations of the deformed hexagon. The explanation is as follows: The 600-nm-thick (Zn,Mg)O buffer relaxes during growth, but becomes differently strained in the plane perpendicular to $\vec{c}$ when cooling the samples down to room temperature due to the different thermal expansion of the substrate parallel (x) and perpendicular (y) to its hexagonal axis $\vec{c}_S$. The difference in the thermal expansion coefficients of sapphire $\Delta\alpha_S = \alpha_y - \alpha_x = -0.8 \times 10^{-6}\ \mathrm{K}^{-1}$ [13] yields, for the temperature change necessary to squeeze the hexagon as observed experimentally, $\Delta T \approx [\tan(\gamma/2)/\sqrt{3} - 1]/\Delta\alpha_S = -400$ K, in good accord with the range covered by the cooling process.

In Fig. 2, the absorption and PL spectra of the MQW are depicted. As shown previously [14], the two features X_A and X_A^- relevant in the present context are due to neutral and negatively charged excitons, respectively, involving a hole from the A subvalence band. Characteristic of the weak-doping regime, the absorption through X^- is markedly smaller than that of the neutral exciton, whereas it dominates the PL because of the effective fusion of free excitons and resident electrons prior to recombination. The prominent difference compared to *c*-plane samples is that the spectra now depend on the orientation of the (linear) light polarization with respect to the substrate axis $\vec{c}_S$, clearly manifesting in-plane optical anisotropy. Again, the polarization properties are confirmed on two further samples with slightly different designs ($x_{\mathrm{Mg}} = 0.14$, $d_w = 2.9$ nm). Also, the onset of the barrier absorption varies in the same way with the linear light polarization (not shown in Fig. 2). The plot of the normalized PL signal of X_A^- and X_A versus the angle between the electric field vector $\vec{E}$ and $\vec{c}_S$ in the inset of Fig. 2 exposes a twofold axis of symmetry. Although all experimental data presented so far are fully consistent with the above invoked strain scenario, alternative mechanisms have to be excluded. One possibility is the quantum confined Pockels effect associated with the presence of piezofields in a QW grown along a polar axis. However, the linear polarization of the barrier absorption as well as the absence of a threefold or even sixfold axis of symmetry [15] rules out a remarkable contribution of this effect. Further, the long-range electron-hole exchange interaction as a frequent source of linear polarization in nanostructures [16] cannot play a leading role as it acts only in the neutral exciton with integer spin, whereas we observe the anisotropy also for the charged exciton of half integer spin.

In the remaining part, we explain the experimental findings in terms of the band states involved in the optical transitions. Our goal is not the calculation of absolute energies of neutral and charged excitons, but to capture the characteristic modifications induced by the anisotropic strain in the QW plane. Thus, the Hamiltonian used for describing the charged

exciton is $H_{X^-} = H_0 - E^b_{X^-} + H_{\rm SO} + H_{\rm strain}$, where $E^b_{X^-}$ is the energy required to dissociate the complex in the exciton and electron. For the neutral exciton, the electron-hole exchange (EHX) interaction has to be additionally accounted for, yielding $H_X = H_0 + H_{\rm EHX} + H_{\rm SO} + H_{\rm strain}$. H_0 contains all contributions acting in the same way on both states, such as hydrostatic strain, QW confinement, and Coulomb interaction. Here, we ignore minor deviations for the different subvalence states. The SO and strain terms are identical in both Hamiltonians as these interactions affect only the hole state. Explicitly, they can be expressed by $H_{\rm SO} = \delta_{\rm SO}/3\,\vec{L}\vec{\sigma}^h$ and $H_{\rm strain} = \delta_{\rm str}(L_x^2 - L_y^2)$, and the exchange interaction reads as $H_{\rm EHX} = \delta_{\rm EHX}/2\,\vec{\sigma}^e\vec{\sigma}^h$ [5,17]. $\vec{L} = (L_x, L_y, L_z)$ is the hole angular momentum operator and $\vec{\sigma}^e$ and $\vec{\sigma}^h$ are the electron and hole spin operators, respectively. $\delta_{\rm str} = C_5^h(\epsilon_{xx} - \epsilon_{yy})$, where ϵ_{xx} and ϵ_{yy} are the components of the strain tensor and C_5^h is the deformation potential, determines the strain difference between the x and y directions. All signs in the above expressions are chosen such that they describe the energy shift of the hole (and not the opposite shift of the valence band states).

Now, we represent the Hamiltonians in terms of the appropriate basis states. For ZnO, it is sufficient to consider only A and B subvalence bands, since the crystal field splitting is much larger than the SO splitting $\delta_{\rm SO}$ and the mutual admixture of the A and C bands is only a few percent [5]. In this approximation, the standard biaxial strain present in the QW as a result of the pseudomorphic growth mode shifts the A and B valence bands by the same amount and can be hence included in H_0. We note that such a simplification is likely inadequate for treating similar effects in GaN QWs. Denoting by $p^{\pm} = (p_x \pm ip_y)/\sqrt{2}$ the p-type hole orbital wave functions with magnetic quantum number $m = \pm 1$ and by $\alpha_{e(h)}$ and $\beta_{e(h)}$ the spin-up and spin-down wave functions of the electron (hole), respectively, the eight relevant neutral exciton states are $|\alpha_e, p^+\alpha_h\rangle$, $|\alpha_e, p^+\beta_h\rangle$, $(|\alpha_e, p^-\alpha_h\rangle + |\beta_e, p^+\beta_h\rangle)/\sqrt{2}$, $|\alpha_e, p^-\beta_h\rangle$, $|\beta_e, p^+\alpha_h\rangle$, $(|\alpha_e, p^-\alpha_h\rangle - |\beta_e, p^+\beta_h\rangle)/\sqrt{2}$, $|\beta_e, p^-\alpha_h\rangle$, and $|\beta_e, p^-\beta_h\rangle$. The irreducible representation of these exciton states (with the included hole state) are $\Gamma_6(\Gamma_9)$, $\Gamma_5(\Gamma_7)$, $\Gamma_2(\Gamma_7)$, $\Gamma_5(\Gamma_9)$, $\Gamma_5(\Gamma_9)$, $\Gamma_1(\Gamma_7)$, $\Gamma_5(\Gamma_7)$, and $\Gamma_6(\Gamma_9)$. For the charged exciton, only the four hole states $|p^+\alpha_h\rangle$, $|p^+\beta_h\rangle$, $|p^-\alpha_h\rangle$, and $|p^-\beta_h\rangle$ with the symmetry Γ_9, Γ_7, Γ_7, and Γ_9 have to be taken into account. It is noteworthy that $H_{\rm strain}$ does not couple the $p_{x,y}$ states of the A and B valence bands to the p_z orbitals constituting dominantly the C band. Finally, the exciton Hamiltonian with all terms determining the exciton fine structure reads as

$$H_X = \begin{pmatrix}
E_0 & 0 & \delta_{\rm str}/\sqrt{2} & 0 & 0 & \delta_{\rm str}/\sqrt{2} & 0 & 0 \\
0 & E_0+\delta_{\rm SO}+\delta_{\rm EHX} & 0 & \delta_{\rm str} & \delta_{\rm EHX} & 0 & 0 & 0 \\
\delta_{\rm str}/\sqrt{2} & 0 & E_0+\delta_{\rm SO} & 0 & 0 & 0 & 0 & \delta_{\rm str}/\sqrt{2} \\
0 & \delta_{\rm str} & 0 & E_0+\delta_{\rm EHX} & 0 & 0 & \delta_{\rm EHX} & 0 \\
0 & \delta_{\rm EHX} & 0 & 0 & E_0+\delta_{\rm EHX} & 0 & \delta_{\rm str} & 0 \\
\delta_{\rm str}/\sqrt{2} & 0 & 0 & 0 & 0 & E_0+\delta_{\rm SO} & 0 & -\delta_{\rm str}/\sqrt{2} \\
0 & 0 & 0 & \delta_{\rm EHX} & \delta_{\rm str} & 0 & E_0+\delta_{\rm SO}+\delta_{\rm EHX} & 0 \\
0 & 0 & \delta_{\rm str}/\sqrt{2} & 0 & 0 & -\delta_{\rm str}/\sqrt{2} & 0 & E_0
\end{pmatrix}, \tag{1}$$

while for the charged exciton it holds:

$$H_{X^-} = \begin{pmatrix}
E_0 - E^b_{X^-} & 0 & \delta_{\rm str} & 0 \\
0 & E_0 - E^b_{X^-} + \delta_{\rm SO} & 0 & \delta_{\rm str} \\
\delta_{\rm str} & 0 & E_0 - E^b_{X^-} + \delta_{\rm SO} & 0 \\
0 & \delta_{\rm str} & 0 & E_0 - E^b_{X^-}
\end{pmatrix}.$$

E_0 is chosen as the energy of the undisturbed $\Gamma_6(\Gamma_9)$ exciton. $\delta_{\rm str}$ couples hole states with opposite m and identical spin orientation. Its value can be estimated from the deformation potential constant $C_5^h = -1.2 \ldots -1.5$ eV [18,19] and the difference $\epsilon_{xx} - \epsilon_{yy} \approx \Delta\alpha_S \Delta T \approx 3 \ldots 6 \times 10^{-4}$ to be about $\delta_{\rm str} = -1$ meV. From magneto-optical studies [14], it is known that the sequence of the Γ_7 and Γ_9 valence bands is inverted in these MQW structures and that the AB splitting is -6 meV, practically not modified with respect to bulk ZnO [5,20]. In the chosen basis set without the C valence band, the splitting has to be identified with $\delta_{\rm SO}$. The exchange splitting between $\Gamma_5(\Gamma_9)$ and $\Gamma_6(\Gamma_9)$ exciton states in bulk ZnO is $\approx$1 meV [5]. To account for a confinement-induced increase, we use here $\delta_{\rm EHX} = 2$ meV.

The results of the diagonalization of H_{X^-} and H_X are summarized in Fig. 3. The position and length of the bars characterize the energy and normalized oscillator strength, respectively, of the resultant eigenstates. In the upper panels (i), the spectra without anisotropic in-plane strain are drawn, while the two lower panels (ii) and (iii) represent the symmetry-reduced situation for the light polarization $\vec{E} \parallel \vec{c}_S$ and $\vec{E} \perp \vec{c}_S$, respectively. For the charged exciton in Fig. 3(a), the photon energy is measured relative to the X_B^- state, i.e., $E(X_B^-) = E_0 - E^b_{X^-}$. It is seen that the anisotropic strain leads only to a weak repulsion of X_A^- and X_B^-, but a strong redistribution of oscillator strength. Whereas the energetically lower X_A^- becomes stronger polarized along $\vec{c}_S$, the opposite holds for X_B^-. The Kramers degeneracy of the half-integer

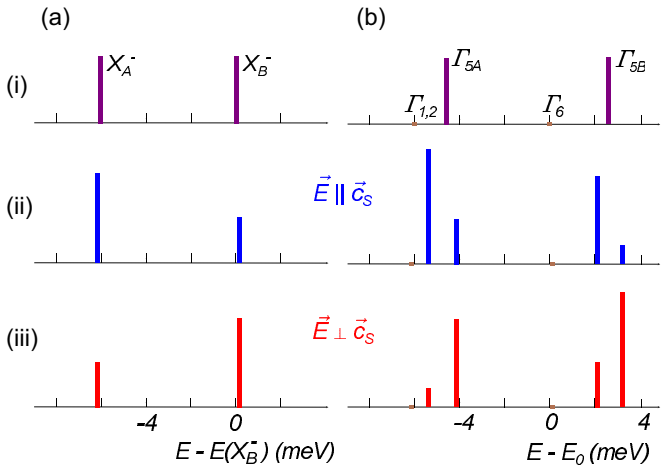

FIG. 3. (Color online) Calculated energy spectrum for the (a) charged and (b) neutral exciton states. The length of the bars represents the normalized oscillator strength for linearly polarized light. (i) Unpolarized spectrum in the case of vanishing anisotropic in-plane strain ($\delta_{\rm str} = 0$). (ii) and (iii) Spectrum for finite strain ($\delta_{\rm str} = -1$ meV) for light polarization $\vec{E} \parallel \vec{c}_S$ and $\vec{E} \perp \vec{c}_S$, respectively.

states cannot be lifted by strain, and instead the hole spin-up and spin-down states are now coupled to orbital states with elliptical symmetry. For example, X_A^- contains the following degenerate, pure spin states: $(0.811p_x - 0.585ip_y)|\alpha_h\rangle$ and $(0.811p_x + 0.585ip_y)|\beta_h\rangle$. The resultant polarization ellipses of opposite rotational sense have identical major axes aligned parallel to $\vec{c}_S$. As generally expected for Kramers-degenerate spin states, there is thus no spin selectivity for linear excitation polarization. For circular polarization, we find a spin excitation degree of $\pm 94\%$ instead of $\pm 100\%$ for $\delta_{\rm str} = 0$. This demonstrates a measurable loss of spin selectivity already at modest anisotropic strain ($\delta_{\rm str}/\delta_{\rm SO} = 0.17$). To achieve full selectivity, elliptic polarization with a major-to-minor axis ratio of about 2:1 has to be used. Larger strain will quickly deteriorate the spin control by circularly polarized photons. The calculated ratio between along and perpendicular to $\vec{c}_S$ polarized X_A^- absorption of $\approx$2:1 agrees fairly well with the experimental data in Fig. 2, proving the correct estimation of the strain difference $\epsilon_{xx} - \epsilon_{yy}$ [21]. It is emphasized that the data again confirm the inverted valence band ordering in ZnO QWs since a positive $\delta_{\rm SO}$ would imply a linear polarization of the X^- transition, just opposite to the experimental findings. The charged exciton PL shows the same preferential linear polarization but with a distinctly smaller intensity ratio. This is expected because the PL intensity only reflects the oscillator strengths if a sufficiently fast relaxation ensures equally populated states. The strain-induced coupling of A and B valence band states in the present QW structures is reminiscent of the heavy-light hole mixing by shape anisotropy in charged quantum dots [22]. In both cases, elliptically polarized transitions occur. However, whereas the orientation of the main axis is fixed for the complete sample in our case, it scatters for the quantum dots.

The EHX interaction present in the exciton results in the slightly more complicated picture shown Fig. 3(b). Since $H_{\rm strain}$ is diagonal with respect to the spin, there is only a coupling between the optical inactive Γ_6 and $\Gamma_{1,2}$ states [23] on the one side and between the Γ_5 states with holes from both subvalence bands on the other side. The latter yields a splitting of both Γ_5 states and polarization-dependent absorption. In contrast to the charged exciton, the degeneracy of these states is lifted and spin superpositions are formed. Although the fine structure of the neutral exciton transition is not completely resolved, a closer inspection of the convoluted band in the absorption spectra of Fig. 2 shows that the experimental data are indeed consistent with the calculated fine structure: The absorption line shapes indicate the contribution of more than the two components (as only found in the case without anisotropic in-plane strain [14]) and the band's center of gravity is located at a lower photon energy for $\vec{E} \parallel \vec{c}_S$. The dependence of the PL intensity on the polarization (Fig. 2 inset) cannot directly correspond to the theoretical oscillator-strength variation as the occupation of the states due to thermalization including the $\Gamma_{1,2}$ states and/or charged-exciton formation is also involved.

In conclusion, the situation of anisotropic in-plane strain in combination with weak SO coupling is studied using the example of a ZnO QW grown on a-plane sapphire. The optical in-plane anisotropy observed for the charged and neutral exciton transitions is qualitatively explained in the frame of the Bir-Pikus Hamiltonian. From the findings, conclusions about the optical spin control can be drawn. For the charged exciton with half-integer spin, the spectrum consist of two spin-degenerate, energetically separated doublets. Pure spin states can be addressed by monochromatic light with properly constructed elliptical polarization. For the neutral exciton states with integer spin, the degeneracy of the optically active Γ_5 states is completely lifted and all of the states no longer represent any pure spin state. GaN QWs are expected to behave similarly, but an adequate description requires here the account of all three subvalence bands. Here, the prerequisite of a crystal field splitting much larger than the SO splitting is not fulfilled [24]. Our results suggest that anisotropic in-plane strain can be utilized for semiconductors with weak SO to tailor the optical spin control in a similar way as biaxial strain allows for the engineering of band masses.

This work was supported by the Deutsche Forschungsgemeinschaft within the Priority program SPP 1285.

[1] C. Klingshirn, Phys. Status Solidi B **244**, 3019 (2007).
[2] T. Dietl, H. Ohno, and F. Matsukura, Phys. Rev. B **63**, 195205 (2001).
[3] *Spin Physics in Semiconductors*, edited by M. I. Dyakonov (Springer, Berlin, 2008).
[4] S. Ghosh, V. Sih, W. H. Lau, and D. D. Awschalom, Appl. Phys. Lett. **86**, 232507 (2005).
[5] J. J. Hopfield, J. Phys. Chem. Solids **15**, 97 (1960); D. G. Thomas, *ibid.* **15**, 86 (1960).
[6] P. Fons, K. Iwata, K. Matsubara, S. Niki, K. Nakahara, T. Tanabe, and H. Takasu, Appl. Phys. Lett. **77**, 1801 (2000).
[7] S. Sadofev, S. Blumstengel, J. Cui, J. Puls, F. Henneberger, R. Schneider, D. Litvinov, and D. Gerthsen, Jpn. J. Appl. Phys. **45**, L1250 (2006).

[8] A. Imamoglu, E. Knill, L. Tian, and P. Zoller, Phys. Rev. Lett. **91**, 017402 (2003).

[9] See, e.g., *Semiconductor Quantum Bits*, edited by F. Henneberger and O. Benson (World Scientific, Singapore, 2008).

[10] S. Sadofev, S. Blumstengel, J. Cui, J. Puls, S. Rogaschewski, P. Schäfer, Y. G. Sadofyev, and F. Henneberger, Appl. Phys. Lett. **87**, 091903 (2005).

[11] K. Vanheusden, C. H. Seager, W. L. Warren, D. R. Tallant, and J. A. Voigt, Appl. Phys. Lett. **68**, 403 (1996).

[12] P. F. Fewster and N. L. Andrew, J. Appl. Crystallogr. **28**, 451 (1995).

[13] W. M. Yim and R. J. Paff, J. Appl. Phys. **45**, 1456 (1974).

[14] J. Puls, S. Sadofev, and F. Henneberger, Phys. Rev. B **85**, 041307(R) (2012).

[15] H. J. Chang, C. H. Chen, L. Y. Huang, and T. Y. Lin, Appl. Phys. Lett. **86**, 011924 (2005).

[16] D. Gammon, E. S. Snow, B. V. Shanabrook, D. S. Katzer, and D. Park, Phys. Rev. Lett. **76**, 3005 (1996).

[17] G. L. Bir and G. E. Pikus, *Simmetrija i Deformacionnye Effekty v Poluprovodnikach* (Izdat. Nauka, Moskow, 1972).

[18] D. W. Langer, R. N. Euwema, K. Era, and T. Koda, Phys. Rev. B **2**, 4005 (1970).

[19] J. Wrzesinski and D. Fröhlich, J. Cryst. Growth **184–185**, 686 (1998).

[20] A. V. Rodina, M. Strassburg, M. Dworzak, U. Haboeck, A. Hoffmann, A. Zeuner, H. R. Alves, D. M. Hofmann, and B. K. Meyer, Phys. Rev. B **69**, 125206 (2004).

[21] The discussion is restricted here to X_A^-. Only this state is resolved in the absorption spectra since the X_B^- transition is covered by the low energy tail of the neutral exciton transitions with much stronger absorption. For PL, X_A^- is only seen due to fast B to A hole relaxation (see Ref. [14]).

[22] A. V. Koudinov, I. A. Akimov, Yu. G. Kusrayev, and F. Henneberger, Phys. Rev. B **70**, 241305(R) (2004).

[23] The weak coupling of the Γ_1 exciton to the optically allowed exciton state with the C band hole not considered here yields a weak absorption for $\vec{E} \parallel \vec{c}$ [5].

[24] B. Gil, O. Briot, and R. L. Aulombard, Phys. Rev. B **52**, R17028 (1995).